Optimizing pump-probe switching ruled by free-carrier dispersion

S. Malaguti,* G. Bellanca, and S. Trillo

Department of Engineering, University of Ferrara, Via Saragat 1, 44122 Ferrara, Italy

*stefania.malaguti@unife.it

Abstract: We address theoretically and numerically pump-probe switching in a nonlinear semiconductor nanocavity where tuning is achieved via a dominant mechanism of free-carrier plasma dispersion. By using coupled-mode approach we give a set of guidelines to optimize the switching performances both in terms of avoiding self-pulsation and keeping switching power to the minimum, ending up by showing that such devices can achieve high-performances with relatively low-power consumption.

OCIS codes: (190.1450) Bistability; (190.4360) Nonlinear optics, devices; (160.5298) Photonic crystals.

References and links

1. T. Tanabe, M. Notomi, S. Mitsugi, A. Shinya, and E. Kuramochi, "Fast bistable all-optical switch and memory on a silicon photonic crystal on-chip," Opt. Lett. **30**, 2575–2577 (2005).
2. M. Notomi, A. Shinya, S. Mitsugi, G. Kira, E. Kuramochi, and T. Tanabe, "Optical bistable switching action of Si high-Q photonic-crystal nanocavities," Opt. Express **13**, 2678–2687 (2005).
3. T. Uesugi, B.-S. Song, T. Asano, and S. Noda, "Investigation of optical nonlinearities in an ultra-high-Q Si nanocavity in a two-dimensional photonic crystal slab," Opt. Express **14**, 377–386 (2006).
4. E. Weidner, S. Combrié, A. de Rossi, N. V. Q. Tran, and S. Cassette, "Nonlinear and bistable behavior of an ultrahigh-Q GaAs photonic crystal nanocavity," Appl. Phys. Lett. **90**, 101118 (2007).
5. S. Combrié, N. V. Q. Tran, A. de Rossi, and H. Benisty, "GaAs photonic crystal cavity with ultrahigh Q: microwatt nonlinearity at 1.55 μm," Opt. Lett. **33**, 1908–1910 (2008).
6. K. Nozaki, T. Tanabe, A. Shinya, S. Matsuo, T. Sato, H. Taniyama, and M. Notomi, "Sub-femtojoule all-optical switching using a photonic crystal nanocavity," Nat. Photonics **4**, 477–483 (2010).
7. K. Nozaki, A. Shinya, S. Matsuo, Y. Suzaki, T. Segawa, T. Sato, R. Takahashi, and M. Notomi, "Ultralow-power all-optical RAM based on nanocavities," Nat. Photonics **6**, 248–252 (2012).
8. Y. Dumeige, and P. Féron, "Stability and time-domain analysis of the dispersive tristability in microresonators under modal coupling," Phys. Rev. A **84**, 043847 (2011).
9. V. Van, T. A. Ibrahim, K. Ritter, P. P. Absil, F. G. Johnson, R. Grover, J. Goldhar, and P.-T. Ho, "All-optical nonlinear switching in GaAs-AlGaAs microring resonators," IEEE Photon. Technol. Lett. **14**, 74–76 (2002).
10. Q. Xu and M. Lipson, "Carrier-induced optical bistability in silicon ring resonators," Opt. Lett. **31**, 341–343 (2006).
11. I. D. Rukhlenko, M. Premaratne, and G. P. Agrawal, "Analytical study of optical bistability in silicon ring resonators," Opt. Lett. **35**, 55–57 (2009).
12. A. Martinez, J. Blasco, P. Sanchis, J. V. Galan, J. Garcia-Ruperez, E. Jordana, P. Gautier, Y. Lebour, S. Hernandez, R. Spano, R. Guider, N. Daldosso, B. Garrido, J. M. Fedeli, L. Pavesi, and J. Marti, "Ultrafast all-optical switching in a silicon-nanocrystal-based silicon slot waveguide at telecom wavelengths," Nano Lett. **10**, 1506–1511 (2010).
13. I. D. Rukhlenko, M. Premaratne, and G. P. Agrawal, "Analytical study of optical bistability in silicon-waveguide resonators," Opt. Express **17**, 22124–22137 (2009).
14. C. Manolatou and M. Lipson, "All-optical silicon modulators based on carrier injection by two-photon absorption," J. Lightwave Technol. **24**, 1433–1439 (2006).
15. A. de Rossi, M. Lauritano, S. Combrié, Q.V. Tran, and C. Husko, "Interplay of plasma-induced and fast thermal nonlinearities in a GaAs-based photonic crystal nanocavity," Phys. Rev. A **79**, 043818 (2009).

#188285 - $15.00 USD Received 3 Apr 2013; revised 5 Jun 2013; accepted 7 Jun 2013; published 25 Jun 2013

16. C. Husko, A. De Rossi, S. Combrié, Q. V. Tran, F. Raineri, and C. W. Wong, "Ultrafast all-optical modulation in GaAs photonic crystal cavities," Appl. Phys. Lett. **94**, 021111 (2009).
17. S. Malaguti, G. Bellanca, A. de Rossi, S. Combrié, and S. Trillo, "Self-pulsing driven by two-photon absorption in semiconductor nanocavities," Phys. Rev. A **83**, 051802(R) (2011).
18. A. Rodriguez, M. Soljačić, J. D. Joannopoulos, and S. G. Johnson, "$\chi(2)$ and $\chi(3)$ harmonic generation at a critical power in inhomogeneous doubly resonant cavities," Opt. Express, **15**, 7303–7318 (2007).
19. K. Ikeda and O. Akimoto, "Instability Leading to Periodic and Chaotic Self-Pulsations in a Bistable Optical Cavity," Phys. Rev. Lett. **48**, 617–620 (1982).
20. B. Maes, M. Fiers, and P. Bienstman, "Self-pulsing and chaos in short chains of coupled nonlinear microcavities," Phys. Rev. A **80**, 033805 (2009).
21. V. Grigoriev and F. Biancalana, "Resonant self-pulsations in coupled nonlinear microcavities," Phys. Rev. A **83**, 043816 (2011).
22. S. Chen, L. Zhang, Y. Fei, and T. Cao, "Bistability and self-pulsation phenomena in silicon microring resonators based on nonlinear optical effects," Opt. Express **20**, 7454–7468 (2012).
23. M. Brunstein, A. M. Yacomotti, I. Sagnes, F. Raineri, L. Bigot, and J. A. Levenson, "Excitability and self-pulsing in a photonic crystal nanocavity, Phys. Rev. A **85**, 031803(R) (2012).
24. T. Van Vaerenbergh, M. Fiers, J. Dambre, and P. Bienstman, "Simplified description of self-pulsation and excitability by thermal and free-carrier effects in semiconductor microcavities," Phys. Rev. A **86**, 063808 (2012).
25. T. Gu, N. Petrone, J. F. McMillan, A. van der Zande, M. Yu, G. Q. Lo, D. L. Kwong, J. Hone, and C. W. Wong, "Regenerative oscillation and four-wave mixing in graphene optoelectronics," Nature Photon. **6**, 554–559 (2012).
26. X. Sun, X. Zhang, C. Schuck, and H. X. Tang, "Nonlinear optical effects of ultrahigh-Q silicon photonic nanocavities immersed in superfluid helium," Sci. Rep. **3**, 01436 (2013).
27. Y. Dumeige, A. M. Yacomotti, P. Grinberg, K. Bencheikh, E. Le Cren, and J. A. Levenson, "Microcavity-quality-factor enhancement using nonlinear effects close to the bistability threshold and coherent population oscillations," Phys. Rev. A **85**, 063824 (2012).

1. Introduction

Nanocavities with high Q/V ratio allows for strong enhancement of nonlinear behavior which has been exploited for achieving ultra-fast switching in different platforms involving, e.g., defects in photonic crystal (PhC) membranes [1–7] or microring resonators [8–11]. Such structures, made either in silicon or III-V semiconductors, have demonstrated the viability of free-carrier dispersion (FCD) induced by two-photon absorption (TPA) as a dominant nonlinear effect [12–14]. In particular, such mechanism permits pump-probe operations, where a carrier-plasma density induced by TPA of a high-intensity pump coupled via a waveguide, causes the refractive index change inside the cavity and, as a consequence, the wavelength resonant tuning of the probe signal [15, 16]. However, switching could be quite demanding in terms of energy consumption, as long as the dynamical pump-probe interaction is not properly designed. Moreover, it has been predicted that the non-instantaneous response of the carriers determines the onset of a FCD-driven instability, namely self-pulsing (SP) [17]. This is an widespread phenomenon first predicted for Kerr-like nonlinearities [19] and recently investigated theoretically and experimentally in different nano-structures [20–26]. In this paper, we give criteria for optimizing bistable pump-probe operations both in terms of minimizing the required switching power and avoiding SP, which could impact the switching dynamics, spoiling the simple bistable features. This is provided by suitable choice of the detunings of the pump-probe pair for a given time constant of carrier dynamics.

2. Coupled-mode equations and lossless dynamics

We start by considering the model for a single slowly-varying envelope analyzed in [15, 17], suitably generalized to account for non-degenerate pump-probe operation occurring in a system composed of a resonator coupled to a waveguide in which the standard Kerr effect is negligible compared to FCD driven by TPA. The model applies to semiconductors where TPA is the main source of losses (e.g., not in the regime considered in [6,7]). By denoting as $a_{p,s}$ the normalized (dimensionless) time-dependent variables that stand for intra-cavity pump and signal (probe)

#188285 - $15.00 USD Received 3 Apr 2013; revised 5 Jun 2013; accepted 7 Jun 2013; published 25 Jun 2013

fields and the carrier density as n, and assuming that $|a_p|^2 \gg |a_s|^2$, which implies that TPA and any related effect such as FCD are essentially driven by the more intense pump field, such model reads as [14]

$$\frac{\partial a_p}{\partial t} = i(\delta_p + n)a_p - a_p - \alpha|a_p|^2 a_p - \gamma n a_p + \sqrt{P_p}, \quad (1)$$

$$\frac{\partial a_s}{\partial t} = i(\delta_s + n)a_s - a_s - 2\alpha|a_p|^2 a_s - \gamma n a_s + \sqrt{P_s}, \quad (2)$$

$$\frac{\partial n}{\partial t} = |a_p|^4 - \frac{n}{\tau}, \quad (3)$$

where the time t and characteristic lifetime of generated carriers τ are in units of $1/\Gamma_0 \equiv 2Q/\omega_0 = 2\tau_0$, where Γ_0 and τ_0 are the field damping coefficient and the cavity lifetime, respectively, ω_0 is the cavity resonance and Q is the quality factor. We also recall that $|a_j|^2, P_j$, $j = p,s$ and n are related to the real-world intra-cavity energy $|U|^2$, input power P_{in}, and carrier density N, as follows: $|a_j|^2 = |U_j|^2\sqrt{\sigma\beta}$, $P_j = (\sqrt{\sigma\beta}/\Gamma_0)(P_{in})_j$, $n = \sigma N$, where $\sigma[m^3] \equiv e^2/(\Gamma_0 2\varepsilon_0 n_0^2 \omega_0 m^*)$ and $\beta[J^{-2}m^{-3}] \equiv c^2\beta_{TPA}/(\Gamma_0 2\hbar\omega_0 n_0^2 V_{TPA}V_{car})$, being c the vacuum light speed, n_0 the refractive index, $\hbar$ the Planck constant, e the electron charge, m^* the electron effective mass, β_{TPA} the TPA coefficient, σ_e and σ_h the cross sections for free-electron absorption and free-hole absorption, respectively, V_{TPA} the nonlinear TPA volume, and V_{car} the volume in which the charges spread and recombine [15]. The important parameters are the cavity detunings $\delta_{p,s} = (\omega_0 - \omega_{p,s})/\Gamma_0$ at pump and probe frequencies $\omega_{p,s}$, respectively, whereas α and γ are the normalized loss coefficients for TPA and free carrier absorption (FCA), whose explicit expressions are reported in [17].

We point out that Eqs. (1)–(3) can be explicitly derived from the following equations for a single envelope at the resonant reference frequency ω_0 (the model in [17] with zero detuning)

$$\frac{\partial a}{\partial t} = ina - a - \alpha|a|^2 a - \gamma n a + \sqrt{P}; \quad \frac{\partial n}{\partial t} = |a|^4 - \frac{n}{\tau}. \quad (4)$$

By inserting in Eqs. (4) the two-frequency ansatz $a = a_p \exp(-i\delta_p t) + a_s \exp(-i\delta_s t)$ and $\sqrt{P} = \sqrt{P_p}\exp(-i\delta_p t) + \sqrt{P_s}\exp(-i\delta_s t)$ and grouping terms with the same frequency, we arrive at Eqs. (1)–(3). We recall that two approximations are essentially involved in this step. The first involves approximating $|a|^4 \simeq |a_p|^4$ in the rate equation for the carrier density, which amounts to assume that the carriers are essentially generated by the pump ($|a_p|^2 \gg |a_s|^2$). The second one involves neglecting the last term in the following expansion of the nonlinear loss term from the first of Eqs. (4): $\alpha|a|^2 a \approx \alpha\left(|a_p|^2 a_p \exp(-i\delta_p t) + 2|a_p|^2 a_s \exp(-i\delta_s t) + a_p^2 a_s^* \exp[-i(2\delta_p - \delta_s)t]\right)$. The latter term is indeed responsible for four-wave mixing, i.e. the generation of a new idler frequency $2\delta_p - \delta_s$ which turns out to be the specular image of the probe frequency with respect to the pump. Such frequency and the consequent modulation impressed on the carriers could be accounted for [27], though only at the expense of adopting a self-consistent model more complicated than Eqs. (1)–(3). In the regime considered here, where the probe beam is brought on resonance by the nonlinear effect, the four-wave mixing frequency turns out to be sufficiently detuned from the resonance, and hence is expected to be negligible (this is especially true in the optimal conditions defined in the analysis reported below). In this case, Eqs. (1)–(3), where only the incoherent nonlinear coupling between the probe and pump beams is retained (as also done in [14]), constitute a satisfactory approximation which allows us to successfully tackle the optimization problem. Note that we retain a factor of two in the cross-TPA nonlinear loss term in Eq. (2) which ultimately stems from the non-degeneracy of the frequencies involved in the underlying nonlinear susceptibility term.

#188285 - $15.00 USD Received 3 Apr 2013; revised 5 Jun 2013; accepted 7 Jun 2013; published 25 Jun 2013

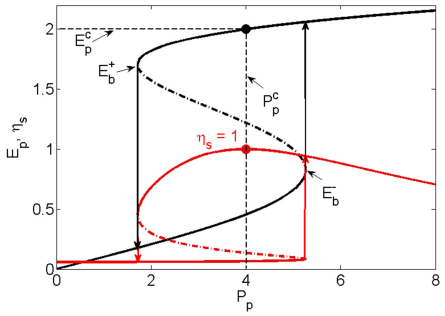

Fig. 1. Typical stationary responses [Eqs. (6)] for pump (E_p vs. P_p, black curve) and probe (η_s vs. P_p, red curve). We highlight the bistable jumps (arrows) occurring at branch point energies $E_b^{\pm}$, and the critical pump point $[P_p^c, E_p^c$, Eq. (7)] for highest probe efficiency $\eta_s = 1$. Dot-dashed portions stand for unstable branches. Here $\delta_p = -3$, $\delta_s = -4$, and $\tau = 1$.

In order to understand the effect of FCD over the pump-probe operation, let us first analyze the dynamics ruled by Eqs. (1)–(3) in the absence of nonlinear losses and FCA (lossless limit) [17]. When the loss coefficients α and γ are set to zero, the system reduces to

$$\frac{\partial a_j}{\partial t} = i(\delta_j + n)a_j - a_j + \sqrt{P_j},\ j = p,s;\ \frac{\partial n}{\partial t} = |a_p|^4 - \frac{n}{\tau}. \tag{5}$$

The corresponding steady-state ($d/dt = 0$), once expressed in terms of probe efficiency $\eta_s = E_s/P_s$, i.e. the cavity energy stored per unit pump power, reads as

$$P_p = E_p\left[1 + (\delta_p + \tau E_p^2)^2\right]\ ;\ \eta_s = \frac{1}{1 + (\delta_s + \tau E_p^2)^2}, \tag{6}$$

where $E_{p,s} \equiv |a_{p,s}|^2$ are henceforth the intra-cavity energies. Figure 1 shows the pump intra-cavity energy E_p and the switching efficiency η_s as functions of the input pump power P_p. Bistability occurs simultaneously for the pump and probe whenever $\delta_p < \delta_p^c \equiv -\sqrt{5}/2$, featuring three different levels of energy for the same input power P_p, when the latter is in the range $P_p^- \le P_p \le P_p^+$. The values $P_p^{\pm} = P_p(E_b^{\mp})$ can be easily calculated through the first of Eqs. (6) from the branch-point energies

$$E_b^{\pm} = \sqrt{\frac{-3\delta_p \pm \sqrt{4\delta_p^2 - 5}}{5\tau}}, \tag{7}$$

which correspond to the knees (branch points) of the bistable response [see Fig. 1]. Figure 1 clearly shows that the bistability of the pump (black curve) drives the probe response (red curve), so that stable (lower and upper) branches of the probe efficiency correspond to stable branches of the pump, whereas the negative-slope (unstable and inaccessible) branch for the probe (dot-dashed in Fig. 1) arises from the similar branch for the pump.

In our analysis, we focus on the pump-probe switch-on regime. This means that the probe is initially blue-detuned from the cavity resonance so that the probe is in a low-state corresponding to $E_s/P_s|_{P_p=0} = (1+\delta_s^2)^{-1} \le 0.5$ (less than 50% of the input is stored in the cavity), which requires to operate with $\delta_s < -1$. Then, the injection of the pump lowers the refractive index, shifting the cavity resonance and inducing the probe beam to jump on a high-state. In particular, our aim is to investigate the conditions to achieve the switching with *Maximal Probe Efficiency*

#188285 - $15.00 USD Received 3 Apr 2013; revised 5 Jun 2013; accepted 7 Jun 2013; published 25 Jun 2013

(MPE) $\eta_s = 1$. By solving $d\eta_s/dE_p = 0$ from the second of Eqs. (6), we find the following expressions for the critical pump energy E_p^c and the corresponding input power P_p^c,

$$(E_p^c)^2 = -\frac{\delta_s}{\tau};\ P_p^c = \sqrt{\frac{|\delta_s|}{\tau}}\left[1+(\delta_p-\delta_s)^2\right]. \tag{8}$$

These critical values identify the point on the pump bistable response such that the injected probe power P_s is switched into the cavity with MPE ($\eta_s = 1$). However since the pump input-output response is multi-valued, in order to understand where the critical operation point is located on the bistable curve, it is important to identify the conditions under which the critical pump energy coincides with the branching points of the response. For a fixed probe detuning δ_s, this occurs at the following values of the pump detuning (obtained by imposing $E_p^c = E_b^{\pm}$)

$$\delta_p^{\pm} = 3\delta_s \pm \sqrt{4\delta_s^2 - 1}. \tag{9}$$

The two values in Eq. (9) along with the threshold value $\delta_p^c \equiv -\sqrt{5}/2$, define three different regimes: (i) $\delta_p^+ \le \delta_p < \delta_p^c$; (ii) $\delta_p^- \le \delta_p \le \delta_p^+$; (iii) $\delta_p \le \delta_p^-$, which correspond to the critical value in Eq. (8) lying on the upper (UB), negative-slope branch, or lower branch (LB) of the three-fold pump response, respectively, yet always maintaining the MPE condition $\eta_s = 1$. On the other hand, another important figure of merit of the probe switch-on is the *Contrast Ratio* (CR) defined as the ratio between the probe energies stored in the resonator in the presence and absence of the pump injection, respectively. For a given probe detuning δ_s, when the condition of MPE is achieved, the CR is calculated to be $1+\delta_s^2 \equiv 1/(\eta_s|_{E_p=0})$, as can be easily obtained from the ratio between the MPE ($\eta_s = 1$) and the value of η_s obtained from the second of Eqs. (6) for $E_p = 0$. Therefore, optimization of the pump-probe switching requires first to choose the value of probe detuning δ_s accordingly with the desired CR, and then to choose the pump detuning δ_p that ensures the MPE with lowest possible pump power.

In order to work out the latter criterium we have summarized the results given through Eqs. (8) and (9) in Fig. 2, which shows a level map of the critical pump power P_p^c in the parameter plane (δ_p, δ_s) with fixed τ, along with samples of pump-probe responses. In Fig. 2(a), the bistable region lying on the left of the vertical dashed line $\delta_p = \delta_p^c$, is divided by the curves $\delta_p^-(\delta_s)$ [solid red] and $\delta_p^+(\delta_s)$ [solid green] into three domains labeled UB, LB, and NSB, according to the name of the branch of the pump response where the critical condition in Eq. (8) falls.

To better illustrate how the MPE and the corresponding critical pump value move on the bistable response, the latter is shown in Figs. 2(b)–2(e) for different (increasing in modulus) values of $\delta_p < \delta_p^c$, and fixed $\delta_s = -3$. As shown in Fig. 2(b), when $\delta_p^+ \le \delta_p < \delta_p^c$, the critical point (8) lies on the UB, and moves together with the MPE condition at lower pump powers for increasing detuning in modulus. Under this regime, the minimum driving pump power needed to yield the MPE condition, is clearly obtained when $P_p = P_p^+$ (i.e., when the cavity is driven at the first knee of the response), which is obtained for $\delta_p = \delta_p^u = -2.2$, as illustrated in Fig. 2(c).

Keeping on increasing $|\delta_p|$ results in further shifting the critical point on the UB of the response. However this does not allow to decrease the minimum required pump power, since these points can be reached only through hysteresis by decreasing P_p after switch-on to the UB, which still requires to drive the cavity above the knee $P_p = P_p^+$. This situation holds up to the limit value $\delta_p = \delta_p^+ = -3.1$ such that the MPE is obtained exactly at the upper knee of the response as shown in Fig. 2(d).

Further increasing $|\delta_p|$ above the value $|\delta_p^+|$ [i.e. entering the region labeled NSB in Fig. 2(a)], makes the critical point (8) to move on the negative-slope branch, thus making the MPE condition unaccessible. This regime holds until $|\delta_p|$ reaches the new limit value $|\delta_p^-|$, in correspondence of which the cavity operates on the first knee of the LB [see Fig. 2(e)]. For detunings

#188285 - $15.00 USD Received 3 Apr 2013; revised 5 Jun 2013; accepted 7 Jun 2013; published 25 Jun 2013

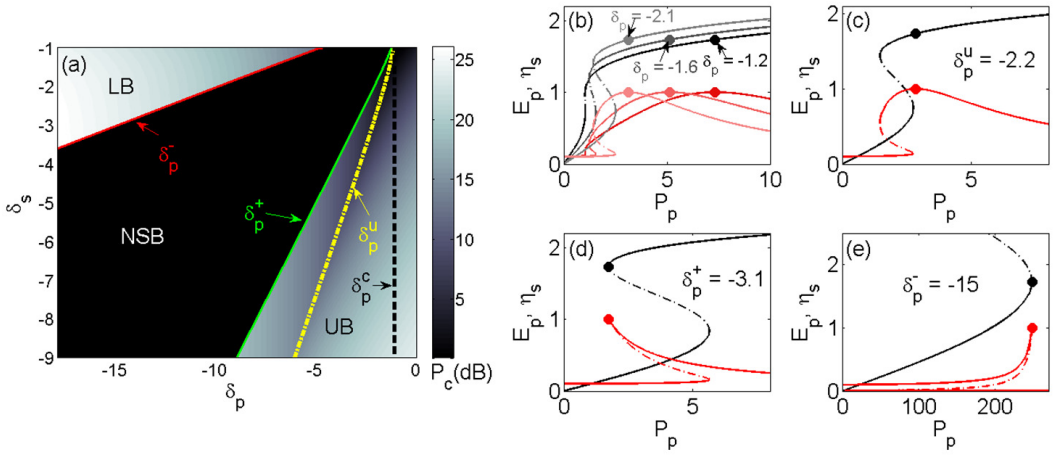

Fig. 2. (a) Level plot of power P_p^c (dB units) from Eq. (8) in the plane of detunings (δ_p, δ_s). In the bistable region (left of the vertical dashed line $\delta_p = \delta_p^c$), the curves labelled δ_p^+ (green) and δ_p^- (red) delimit the domains corresponding to the three branches of the stationary response shown in Fig. 1 (LB/UB stand for the lower/upper branch, NSB stands for the negative-slope branch). The optimum (MPE $\eta_s = 1$ with minimal P_p) is achieved for pump detunings δ_p^u (yellow dot-dashed curve). (b)-(e) Corresponding steady-state pump (black) and probe efficiency (red) responses for fixed probe detuning $\delta_s = -3$ ($CR = 10$) and increasing values of $|\delta_p|$. The dots indicate the optimum operation points (the red and black dots give MPE $\eta_s = 1$ and corresponding critical values $P_p = P_p^c, E_p = E_p^c$, respectively): (b) Pump detuning values $\delta_p = -1.2, -1.6, -2.1$ ($P_c = 7.3, 5.1, 3.1$) in the UB region; (c) Optimum operation at $\delta_p = \delta_p^u = -2.2$ (minimal $P_p^c = 2.8$); (d)-(e) MPE at $\delta_p^+ = -3.1$ and $\delta_p^- = -15$, respectively. Here $\tau = 1$.

$|\delta_p| \geq |\delta_p^-|$, the MPE condition becomes accessible again since the critical point (8) lies on the LB, though the required input powers grow so large to become unpractical, as can be clearly seen in Fig. 2(e).

Therefore we conclude that optimized pump-probe operation which allows to obtain MPE with minimal pump power requires to operate at the pump detuning $\delta_p = \delta_p^u$ such that the critical point coincides with the UB energy level [black dot in Fig. 2(c), not to be confused with E_b^- in Eq. (7)] that corresponds to the knee level of input power $P_p = P_p^+$. This optimum detuning can be found for any choice of the signal detuning δ_s by imposing that the largest real root $E_p = E_p(P_p^+)$ coincides with the critical value $E_p^c = \sqrt{-\delta_s/\tau}$. The pump detunings δ_p^u that fulfills this constraint (no simple analytical expression can be found since it involves the roots of a quintic polynomial) for different values of probe detuning δ_s, leads to the curve of optimal detunings reported (in dot-dashed yellow line) in the parameter plane in Fig. 2(a). The choice of δ_p on this curve guarantees to reach the MPE condition with minimal required pump power.

It is worth noting that the curves delimiting the different regions in Fig. 2(a) remain unchanged with respect to variations of τ. This means that for fixed δ_s (fixed CR), by varying τ, the pump power level needed to obtain MPE changes, but the required value δ_p^u is the same in the same cavity, regardless of the specific carrier lifetime.

#188285 - $15.00 USD Received 3 Apr 2013; revised 5 Jun 2013; accepted 7 Jun 2013; published 25 Jun 2013

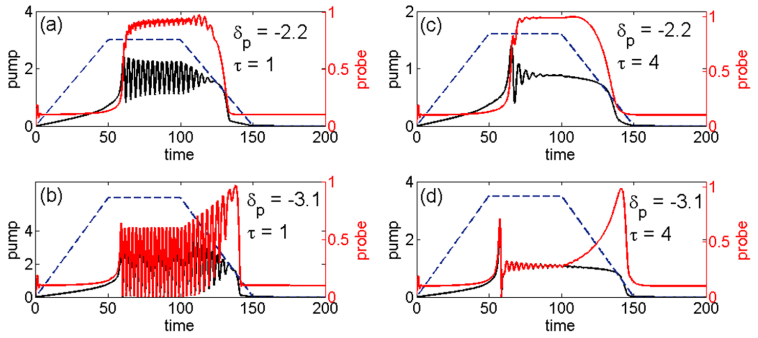

Fig. 3. Temporal dynamics of pump (solid black) and probe (solid red) energies for $\delta_s = -3$ and pump detuning: (a)-(c) $\delta_p = -2.2$ (peak power $P_p = 3$); (b)-(d) $\delta_p = -3.1$ (peak power $P_p = 6$). The left column cases (a)-(b) and right column cases (c)-(d) are relative to $\tau = 1$ and $\tau = 4$, respectively. The (blue) dashed line is the driving pump $P_p(t)$ (P_s is a cw signal).

3. Role of self-pulsing

The analysis of the previous section is based on the stationary response. However, as shown previously in [17], FCD with finite lifetime of the carriers can be responsible for the destabilization of the UB steady-states via a Hopf bifurcation, which causes the onset of spontaneous oscillations (SP). As long as $|a_p|^2 \gg |a_s|^2$, SP is induced by the pump and its threshold analysis carried out in [17] remains valid. Here, in order to investigate how SP affects the probe switching, we have integrated numerically Eqs. (5). We report examples for the case in which the probe is a cw signal, whereas the control beam is ramped slowly up and down, following a trapezoidal waveform with given peak value P_p (qualitatively similar results are obtained also for other waveforms).

In Figs. 3(a)-(b) we compare the pump-probe temporal dynamics corresponding to the steady-states displayed in Fig. 2(c) for $\delta_p = -2.2$ and Fig. 2(d) for $\delta_p = -3.1$ (with fixed $\delta_s = -3$, $\tau = 1$). In both cases the up-switching of the pump to the UB, which occurs at peak value P_p (we use $P_p = 3, 6$ for $\delta_p = -2.2, -3.1$), always triggers the onset of SP. However, in the optimal case $\delta_p = \delta_p^u = -2.2$, when the pump starts to exhibit SP, the probe has nearly reached the MPE condition in up-switching and shows only small spurious oscillations driven by those of the pump beam. Therefore SP does not dramatically deteriorate the probe switching performances. Conversely, the case $\delta_p = -3.1$ (non-optimal detuning), besides requiring a nearly double power P_p, leads to a dynamics where strong oscillations are exhibited by both beams. In this case SP heavily affects the dynamics of the probe over the whole signal duration, up to the MPE point $\eta_s \sim 1$, which is reached only in a particular instant when the pump experiences down-switching [as expected from Fig. 2(d)].

The SP, however, is greatly affected by the carrier lifetime, and can be inhibited by τ large enough [17]. This is illustrated in Figs. 3(c)-3(d), where we display the dynamics obtained with $\tau = 4$, while the detunings are the same as in Figs. 3(a)-3(b). In this case no SP occurs and the pump dynamics shows only strongly damped relaxation oscillations that are characteristic of any bistable system. With optimal detuning [$\delta_p = -2.2$, Fig. 3(c)], the MPE is reached in up-switching and maintained until the pump ramps down, whereas for $\delta_p = -3.1$ [Fig. 3(d)], MPE is reached again only in down-switching.

In terms of typical dimensional quantities that correspond to pump-probe experiments performed in III-V photonic crystal cavities [15, 16], operating with $\tau = \tau_r/\tau_0 = 1$ and $\tau_r = 8$ ps amounts to have (at telecom wavelength $\lambda_0 = 1.55$ μm) $Q \simeq 5000$. The dynamics in Fig. 3(a)-

#188285 - $15.00 USD Received 3 Apr 2013; revised 5 Jun 2013; accepted 7 Jun 2013; published 25 Jun 2013

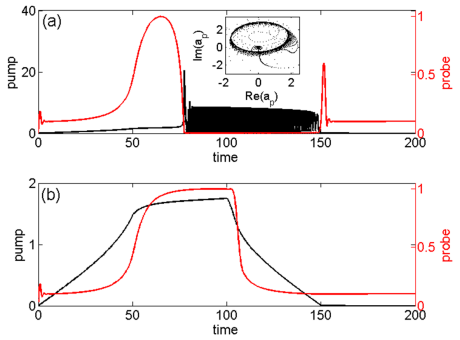

Fig. 4. As in Fig. 3 for $\delta_s = -3$, $\delta_p = -15$, and $\tau = 1$, contrasting two dynamical behaviors: (a) pump self-switching (dark curve) towards a SP state [the inset shows the corresponding limit cycle in the phase plane $\mathrm{Re}(a_p) - \mathrm{Im}(a_p)$], obtained with maximum driving power $P_p = 250$ (slightly larger than knee value P_p^+); (b) stable behavior for $P_p = 248.5$ (slightly lower than P_p^+), with MPE reached with pump on the lower branch (note the different vertical scale in the two plots).

3(b) can be observed by operating with the following dimensional detunings: $\Delta\lambda_s = -0.465$ nm ($\delta_s = -3$), and $\Delta\lambda_p = -0.341$ nm ($\delta_p = -2.2$) or $\Delta\lambda_p = -0.481$ nm ($\delta_p = -3.1$), respectively. The injected powers turns out to be $P_{in} = 2$ mW and $P_{in} = 4$ mW, respectively. With the same carrier lifetime $\tau_r = 8$ ps, $\tau = 4$ [Fig. 3(c)-3(d)] can be obtained by lowering the quality factor to $Q = 1200$, while the detuning values and powers become in this case: $\Delta\lambda_s = -1.937$ nm, $\Delta\lambda_p = -1.421$ nm and $P_{in} = 17.25$ mW ($\delta_p = -2.2$), or $\Delta\lambda_p = -2$ nm and $P_{in} = 37.73$ mW ($\delta_p = -3.1$).

For completeness, we have also investigated the temporal dynamics corresponding to the case in Fig. 2(e), namely for pump detunings so large ($\delta_p = -15$) that the MPE is obtained at a critical energy coincident with the first knee of the response [$E_c \equiv E_b^-$]. For such large values of $|\delta_p|$, when the driving power is slightly higher than the value P_p^+ of the knee, the cavity dynamics is ruled by the up-switching of the pump to the upper branch, which then undergoes SP. This is illustrated in Fig. 4(a) for $\delta_p = -15$ and $P_p = 250$ (corresponding in real-world units to $\Delta\lambda_p = -2.31$ nm and pump power $P_{in} = 168.4$ mW), and $\tau = 1$. As shown, the pump undergoes SP, and its evolution is attracted in phase space towards a stable limit cycle (supercritical Hopf bifurcation). In this case, the onset of SP deteriorates the pump-probe operations by inducing an abrupt switch-off of the probe, which remains in a low state (very far from MPE). Conversely, even a slight decrease of pump power, as shown in Fig. 4(b) for a driving level $P_p = 248.5$ ($P_{in} = 167.4$ mW) leaves the intra-cavity pump on the lower branch, thus allowing for the probe to switch-on and achieve dynamically MPE when the pump reaches its maximum level of intra-cavity energy (yet on the lower branch). This regime, however, is not advantageous due to the large driving power P_p required to reach the MPE.

4. Effect of Losses

In this section we extend the previous analysis to include the effect of losses. Specifically we investigate the effect of TPA losses assuming for simplicity negligible FCA ($\gamma = 0$, though similar qualitative conclusions can be applied to the effect of FCA when is not negligible). While TPA is unavoidable being at the origin of FCD, a proper engineering of the cavity allows for working with relatively low normalized coefficients in the range $\alpha = 0.1 - 0.2$ (see [17] for a discussion). In this case, the steady-state solutions read as ($\eta_s = E_s/P_s$ is the probe switching

#188285 - $15.00 USD Received 3 Apr 2013; revised 5 Jun 2013; accepted 7 Jun 2013; published 25 Jun 2013

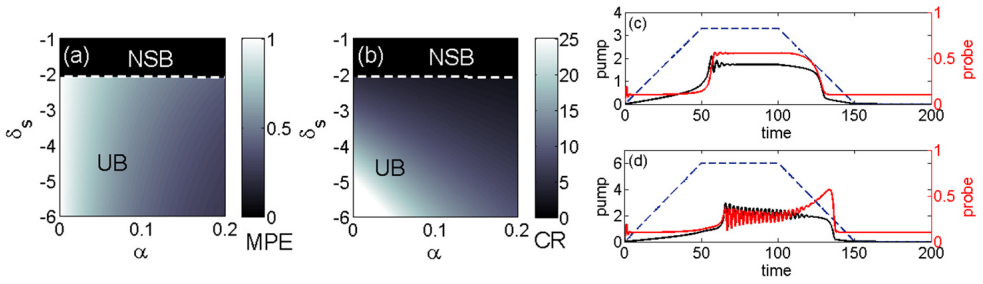

Fig. 5. Effect of TPA: level plots of (a) MPE; (b) CR, in the plane (α, δ_s) for fixed optimum value of pump detuning ($\delta_p^u = -2.2$) and $\tau = 1$ (labels UB and NSB stand for uppe and negative slope branch, respectively). (c)-(d) Temporal pump-probe dynamics for $\alpha = 0.1$ and $\tau = 1$, contrasting: (c) stable probe switching for $\delta_p = -2.2$ (MPE of 0.55 and a CR of 5.5) and (d) SP-dominated dynamics for $\delta_p = -3.1$.

efficiency defined previously)

$$P_p = E_p\left[(1+\alpha E_p)^2 + (\delta_p + \tau E_p^2)^2\right], \quad \eta_s = \frac{1}{(1+2\alpha E_p)^2 + (\delta_s + \tau E_p^2)^2}. \tag{10}$$

Following the approach used for the lossless regime, we first seek for the critical pump energy E_p^c and pump power P_p^c that gives the MPE condition by solving the equation $d\eta_s/dE_p = 0$. In this case, the solution of such equation, as well as the branch-point (knee) energies $E_b^{\pm}$ can be obtained only numerically. The constraint $E_p^c = E_b^{\pm}$ allows us to implicitly draw the threshold curves $\delta_p^{\pm}$ which defines the three regions where MPE occurs on the upper, lower, or negative-slope branch of the bistable response, respectively. Since TPA losses do not significantly affect the branch-point energies, the map of Fig. 2(a) remains practically unchanged (we do not report such map for the lossy case because differences are barely noticeable). Conversely, the losses may significantly affect both the MPE [max(η_s)] and the contrast ratio CR, which are mapped in Figs. 5(a)-5(b) in the plane (α, δ_s) for fixed $\delta_p = -2.2$ and $\tau = 1$. As shown, both the MPE and CR decreases, as expected, for larger losses, while they slightly depend on δ_s.

Based on such maps one can still optimize the pump-probe switching. For instance, with $\tau = 1$ and $\alpha = 0.1$, the choice of probe detuning, for instance $\delta_s = -3$, fixes the contrast ratio to CR$=$ 5.5 from Fig. 5(b). Then the optimum pump detuning remains, with good approximation, unchanged with respect to the lossless case ($\delta_p = -2.2$), whereas the MPE obtained with such detuning, decreases to ~ 0.55 as inferred from Fig. 5(a). The outcome of the numerical integration of Eqs. (1)-(3) reported in Fig. 5(c) confirms such values of MPE and CR. Moreover, comparing with the lossless case in Fig. 3(a), we notice that SP is suppressed. Indeed the TPA losses moves the SP pump energy threshold at a value ($E_H = 1.9$, from the linearized analysis in [17]) larger than the value of the jump on the UB ($E = 1.65$). Therefore we can summarize by saying that the losses on one hand decrease the achievable MPE, and on the other hand stabilize the dynamics against SP even for low values of τ. However the latter statement is true only for the optimum detuning. Non-optimal values of detunings, as shown for instance in Fig. 5(d) for $\delta_p = -3.1$ [comparable with the lossless case in Fig. 3(b)], still leads to SP, besides reaching a reduced MPE in down-switching.

It is important to make two final considerations on the additional losses that can ultimately deteriorate pump-probe switching operations. First, losses due to free-carrier absorption are expected to further reduce the switching performances. For instance, by setting $\gamma = 0.1$ [17], we find that the MPE and the CR are degraded to the values 0.37 and 3.7, respectively. We

#188285 - $15.00 USD Received 3 Apr 2013; revised 5 Jun 2013; accepted 7 Jun 2013; published 25 Jun 2013

point out, however, that, though TPA and FCA losses cannot be completely ignored, they can be significantly reduced by suitable engineering of the material and cavity design. A second issue is related to the regime of operation that involves high repetition rates, which may result in additional losses due to a steady-state component of the carriers. In order to address this issue we carried out simulations for $\delta_p = -2.2$, $\delta_s = -3$, and $\tau = 1$, with $\tau_r = 8$ ps, by considering a RZ train of super-Gaussian pulses, at 2 GHz and then at 12.5 GHz. While at 2 GHz we observe only a slight reduction ($\sim 10\%$) in the MPE and CR (both in the lossless-limit case or accounting for losses), at the higher repetition rate of 12.5 GHz, we find a strong reduction ($\sim 45\%$) in the MPE and CR. Therefore we conclude that, as expected, high repetition rates result in the deterioration of the switching performances.

5. Conclusions

In summary, the analysis of CME for pump-probe operation in a semiconductor nanocavity allows us to assess the optimized conditions for pump-induced switching of the probe beam. For a given desired contrast ratio, the optimization in terms of reaching the best probe efficiency with minimum driving pump power requires the proper choice of the pump detuning, while a constraint on the characteristic lifetime of the carriers is necessary to avoid self-pulsing.

Acknowledgments

This work has been supported by the 7th framework of the European Commission through the COPERNICUS (www.copernicusproject.eu) project.

#188285 - $15.00 USD Received 3 Apr 2013; revised 5 Jun 2013; accepted 7 Jun 2013; published 25 Jun 2013